# Measurement of flow velocity field in corona discharge radical shower non–thermal plasma reactor

J. Dekowski, J. Mizeraczyk

*Centre for Plasma and Laser Engineering, The Szewalski Institute of Fluid Flow Machinery,//Polish Academy of Sciences, Fiszera 14, 80–231 Gdask, Poland*

T. Ohkubo, S. Kanazawa

*Department of Electrical and Electronic Engineering, Oita University, 700 Dannoharu, Oita, Japan 870–1192*

J. S. Chang

*Department of Engineering Physics, McMaster University, Hamilton, Ontario, Canada L8S 4L7*

Received 29 April 2004

In this paper results of the Particle Image Velocimetry (PIV) measurements of the flow velocity fields in a corona discharge radical shower (CDRS) non–thermal plasma reactor are presented. The discharge electrode of the CDRS reactor was a thin tube with several nozzles, through which a gas mixture was added to the reactor. The velocity fields were measured in two flow planes perpendicular to the electrode tube: the first plane was set between two nozzles in the middle of the discharge electrode, and the second passed through one of them. In both planes electrohydrodynamically generated vortexes were found. However, in the plane set between the two nozzles, the vortexes were smaller. This investigation shows that in the reactor with the CDRS discharge electrode is used, the vortexes revolve in the opposite direction to those generated in the non–thermal plasma reactors with smooth wire discharge electrodes. The flow patterns in the reactor with CDRS electrode are more stable than those with the smooth wire electrode. This can have an influence on the performance of the CDRS reactors.

*PACS*: 52.30.Cv
*Key words*: electrohydrodynamic flow, corona discharge radical shower, particle image velocimetry

## 1 Introduction

Non–thermal plasma techniques [1], [2], [3] have become an important tool for controlling the emission of various gaseous pollutants, such as acid gases ($SO_x$, $NO_x$, HCl, etc.), greenhouse gases ($CO_x$, $N_xO_y$, para–fluorocarbons, etc.), ozone depletion gases (freons, halons, etc.), volatile organic compounds (VOCs, e.g. toluene, xylene, etc.) and toxic gases (Hg, dioxins, etc.). The main advantages of the non–thermal plasma techniques are small space volume, low cost, high pollutant removal and energy efficiencies.

CDRS reactors have been recently proved to be one of the most efficient non–thermal plasma reactor systems used for $NO_x$ removal [4], [5], [6]. In a CDRS reactor, a tubular electrode with one or several nozzles is used for additional gas ($NH_3$, $CH_4$, etc.) injection across the corona discharge zone into the main flue gas flow. Due to the additional gas injection the corona discharge produces active species such as NH, $NH_2$, CH, $CH_2$, etc.,

which enhance the removal of $NO_x$. The performance of the CDRS reactors can be also improved by the transport of the long–life species, caused by the electrohydrodynamic (EHD) secondary flow, as it was suggested in [7].

This investigation concerns the measurements of flow velocity field in a CDRS non–thermal plasma reactor using the PIV method [8]. Collecting such data is important for designing the non–thermal reactors of high performance efficiency.

## 2 Experimental apparatus

A schematic of the experimental apparatus used for the measurement of the flow velocity fields in the CDRS reactor is shown in Fig. 1. The reactor was an acrylic box of a rectangular geometry (100 mm × 200 mm × 1000 mm) as used by Mizeraczyk et al. [7]. A stainless–steel tube (4 mm in diameter) with 18 stainless–steel nozzle electrodes (1.5 mm outer diameter, 1 mm inner diameter, 5 mm length), soldered into the tube, was used as the CDRS electrode. It was placed in the middle of the reactor, in the halfway between two grounded parallel plate electrodes (200 mm × 600 mm). Positive polarity DC high voltage was applied through a 10 MΩ resistor to the CDRS electrode. The operating voltage was varied from 0 to 31 kV to develop a stable streamer corona discharge from each electrode nozzle to the plate electrodes. The discharge was operated at room temperature under atmospheric pressure.

Two flows, the main and the additional, were established in the reactor. The main gas (ambient air) flowed along the reactor, driven by an induced fan. The mean velocity of the main gas flow was varied from $U_s = 0$ to $U_s = 0.8\ \mathrm{m\,s^{-1}}$, which corresponds to the flow change from laminar to transitional (Reynolds number varied from Re = 600 to 2660 for $U_s = 0.18\ \mathrm{m\,s^{-1}}$ and $U_s = 0.8\ \mathrm{m\,s^{-1}}$, respectively). The standard deviation of the main gas mean velocity was ± 4 %, as measured with the PIV. The additional gas ($N_2 : O_2 : CO_2$=80 % :5 % :15 %) was injected through the nozzles into the main gas flow with a flow rate varied from 0.25 to $1.5\ \mathrm{l\,min^{-1}}$ (nozzle outlet gas velocity ranged from 0.3 to $1.8\ \mathrm{m\,s^{-1}}$, corresponding to Re = 30 – 180, respectively). The presence of $CO_2$ (15 %) stabilized streamer corona discharge mode, preventing glow and spark discharge modes [9].

The flow velocity fields in the CDRS reactor were measured using the PIV method. The PIV equipment consisted of a twin second harmonic Nd–YAG laser system ($\lambda$ = 532 nm, pulse energy 50 mJ), imaging optics (cylindrical telescope), CCD camera, image processor (Dantec PIV 1100) and PC computer (Fig. 1). A laser sheet of thickness of 1 mm, formed from the Nd–YAG laser beam by the cylindrical telescope, was introduced into the CDRS reactor as a plane perpendicular to the CDRS electrode. The measurements were performed in two different planes, set perpendicularly to the electrode tube; the first plane passed through the central nozzle, and the second passed the halfway between the central and neighbouring electrodes. Seed particulate (cigarette smoke), being expected to follow the flow, was added to the main gas for scattering the laser–sheet light. The particle images were recorded by the Kodak Mega Plus ES 1.0 CCD camera, which could capture two images with a minimum time separation of 2 μs. The CCD camera active element size was 1008 × 1018 pixels. The captured images were transmitted by the Dantec PIV 1100 image

processor to the PC computer for digital analysis to obtain the velocity field maps.

We assumed that the flow in the CDRS reactor is symmetric regarding the horizontal plane (parallel to the plate electrodes) passing through the discharge electrode. Therefore, in this experiment the PIV measurement area was limited to the lower half of the CDRS reactor.

The velocity field maps presented in this paper are composed of 2 or 4 adjacent velocity fields, each of an area of 75 mm × 75 mm. Since it was found in this experiment that the flow structure pattern in the CDRS reactor is unsteady, majority of the velocity field maps resulted from the averaging of 100 measurements, i.e. the presented velocity maps are time–averaged.

## 3 Results

The flow velocity field patterns in the CDRS non–thermal plasma reactor for four different time–averaged velocities of the main flow (0 $m\,s^{-1}$, 0.2 $m\,s^{-1}$, 0.4 $m\,s^{-1}$ and 0.6 $m\,s^{-1}$) at a constant discharge current of 150 μA and an additional flow through the nozzles of 0.5 $l\,min^{-1}$ are shown in Figs. 2 – 5. The patterns concern the two planes: the first plane passing through the central nozzle, and the second passing the halfway between the central and neighbouring electrodes.

The results of the PIV measurements presented in Figs. 2 – 5 show existence of strong EHD secondary flows in the CDRS reactor. As seen from the figures, the secondary flow patterns depend on average velocity of the main flow.

Surprisingly, the direction of rotation of the electrohydrodynamically caused vortexes is opposite to that observed in the ESP with smooth wire discharge electrode [10]. As seen in Figs. 2 – 5, the seed particle flow in the vortexes near the CDRS nozzle electrode moves from the nozzle first against or along the main flow, than turns towards the plate electrodes, and eventually returns to the discharge electrode. This is in contrary to the rotation of the vortexes when the smooth wire electrode is used. In such a case, the seed particles begin their motion from the smooth wire electrode directly towards the plate electrodes, and then they turn to return to the wire electrode. As a result, the near discharge electrode vortexes revolve in the opposite direction to that for the CDRS electrode case found in this investigation.

Without the main flow, strong vortexes are formed upstream and downstream from the discharge electrode (Figs. 2 a and b). The velocity of the additional gas flowing out of the nozzles is about 0.6 $m\,s^{-1}$ (calculated and measured by the PIV). Reynolds number of the jet from the nozzle is about Re = 59 and the EHD number for the nozzle outlet is $E_{hd} = 2.6 \times 10^6$ [11]. Therefore, the flow in the vicinity of the nozzle, resulting in the strong vortexes, is dominated by the EHD forces (the ratio of the EHD number to Reynolds number squared $E_{hd}/Re^2 = 760$). As seen from (Figs. 2 a and b), the flow velocity in the vortexes in the plane passing through the discharge nozzle is higher than that in the plane between the two nozzles. This is brought about by the stronger EHD forces in the plane passing through the nozzle.

At a relatively low main flow velocity of 0.2 $m\,s^{-1}$ (i.e. at a moderate Reynolds number, Re = 663), also strong vortexes are formed in both the upstream and downstream area of the

discharge electrode (Figs. 3 a and b). The vortexes upstream from the discharge electrode become to be shrunk by the main flow. At the primary flow velocity of 0.2 $m\,s^{-1}$, still the electric force is dominating over the inertial one (the EHD number for the area of 10 cm around the discharge electrode is $E_{hd} = 8.5 \times 10^6$, while the ratio $E_{hd}/Re^2 = 19$). However, at this relatively low value of $E_{hd}/Re^2$ there are no significant differences between the flow patterns in the both measurement planes, the one passing through the nozzle and the passing the halfway second between the two nozzles. It is seen from (Figs. 3 a and b) that the main flow is blocked by the EHD forces in the middle of the duct.

The increase in the main flow velocity to $0.4 \div 0.6\ m\,s^{-1}$ diminishes the influence of the electric force on the particle and main flow motions, especially in the plane between the nozzles where the EHD forces are weaker. The vortexes at the upstream side of the discharge electrode become clearly smaller. The main flow, still influenced by the EHD secondary flow, first passes between the upstream vortexes and the plates, then it goes towards the discharge electrode, and eventually passes between both downstream vortexes along the middle of the duct. At the main flow velocity of 0.4 $m\,s^{-1}$ ($Re = 1325$, $E_{hd}/Re^2 = 4.9$) the upstream vortexes shrink slightly (Figs. 4 a and b), but at 0.6 $m\,s^{-1}$ ($Re = 1988$, $E_{hd}/Re^2 = 2.2$) the upstream vortexes become about 3 times smaller than the downstream vortexes (Figs. 5 a and b). At the main flow velocities of 0.4 and particularly at 0.6 $m\,s^{-1}$ the upstream vortexes in the plane between the nozzles are smaller than those in the plane passing through the nozzle.

## 4 Conclusions

The presented results confirmed that the EHD secondary flow in the form of vortexes having velocity of several tens of $cm\,s^{-1}$ are formed in the downstream and upstream region of the CDRS non–thermal plasma reactor, interacting with the main flow.

In this investigation it was found that when the CDRS discharge electrode is used, the vortexes generated by the EHD forces revolve in the opposite direction to the vortexes generated in the non–thermal plasma reactors with the smooth wire discharge electrode. Besides, the flow structures in the CDRS reactor are more stable than those in the reactors with smooth wire electrodes.

The results show differences in the flow velocity field patterns in the plane passing through the discharge nozzle and those in the plane passing between the nozzles. The vortexes observed in the plane between the nozzles are smaller than those in the plane passing through the nozzle. This is caused by the weaker EHD forces in the plane passing in the halfway between the nozzles. The difference in the vortex sizes is more pronounced for higher main flow velocities.

This investigation shows that the distance between discharge nozzles has significant impact on the flow structures in CDRS reactors when higher main flow velocities are used.

This work was supported by the Foundation for Polish Science (FNP, subsidy 8/2001) and the Institute of Fluid Flow Machinery (grant IMP PAN O3/Z–3/T2).

## References


[1] J. S. Chang, P. Lawless, T. Yamamoto: *Corona Discharge Processes*, IEEE Plasma Sci. **19** (1991) 1152–1166.

[2] B. M. Penetrante, J. N. Bardsley, M.C. Hsiao: *Kinetic Analysis of Non–thermal Plasmas Used for Pollution Control*, J. Appl. Phys. **36** (1997) 5007–5017.

[3] K. Urashima, J. S. Chang: *Removal of Volatile Organic Compounds from Air Streams and Industrial Flue Gases by Non–thermal Plasma Technology*, IEEE Trans. Dielectrics and Electrical Insulation **7** (2000) 602–614.

[4] T. Ohkubo, S. Kanazawa, Y. Nomoto, J. S. Chang, T. Adachi: *$NO_x$ Removal by a Pipe with Nozzle–Plate Electrode Corona Discharge System*, IEEE Trans. Ind. Appl. **30** (1994) 856–861.

[5] S. Kanazawa, J. S. Chang, G. F. Round, G. Sheng, T. Ohkubo, Y. Nomoto, T. Adachi: *Removal of $NO_x$ from Flue Gas by Corona Discharge Activated Methane Radical Showers*, J. Electrostatics **40&41** (1997) 651–656.

[6] K. Urashima, S. J. Kim, J. S. Chang: *The Scale–up and Economic Evaluation of Non–thermal Plasma Technology for Coal Fired Power Plant Exhaust Gas Emission Control*, J. Adv. Oxid. Tech. **6** (2003) 123–131.

[7] J. Mizeraczyk, J. Podliski, M. Dors, M. Kocik, T. Ohkubo, S. Kanazawa, J. S. Chang: *Electrohydrodynamic Transport of Ozone in a Corona Radical Shower Non–thermal Plasma Reactor*, Czech. J. Phys. **52** Suppl. D (2002) 413–420.

[8] J. Westerweel: *Fundamentals of Digital Particle Image Velocimetry* , Meas. Sci. Technol. **8** (1997) 1379–1392.

[9] K. Yan, T. Yamamoto, S. Kanazawa, T. Ohkubo, Y. Nomoto, J. S. Chang: *Control of Flow Stabilized Positive Corona Discharge Modes and NO Removal Characteristics in Dry Air by $CO_2$*, J. Electrostatics **46** (1999) 207–219.

[10] J. Mizeraczyk, M. Kocik, J. Dekowski, M. Dors, J. Podliski, T. Ohkubo, S. Kanazawa, T. Kawasaki: *Measurement of the velocity field of the flue gas flow in an electrostatic precipitator model using PIV method*, J. Electrostatics **51–52** (2001) 272–277.

[11] J. S. Chang, A. Watson: *Electromagnetic Hydrodynamics*, IEEE Trans. Dielectrics and Electrical Insulation **5** (1994) 871–895.

## 5 Figures

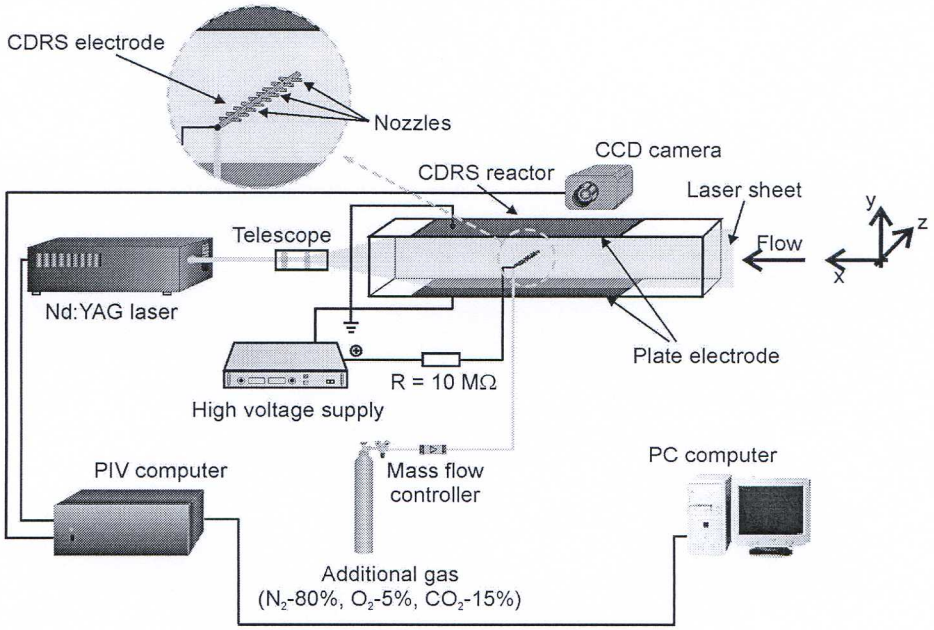


Fig. 1. Experimental set–up.

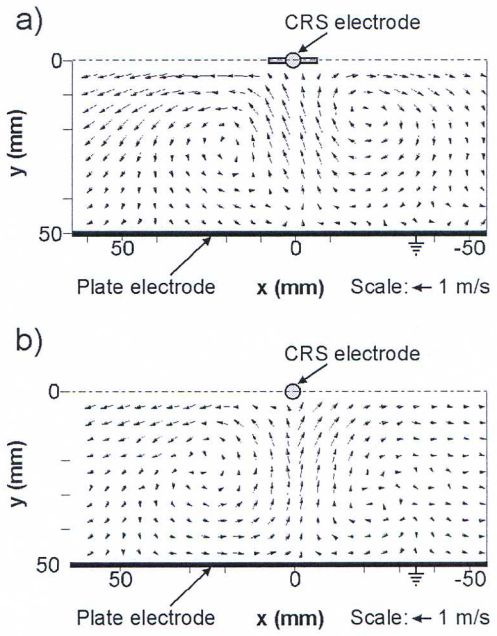


Fig. 2. Flow velocity field in the CDRS non–thermal plasma reactor without main flow. Positive polarity, discharge current 150 μA, additional gas flow 0.5 $l\,min^{-1}$. a) the observation plane through the nozzle, b) the observation plane between the two nozzles.

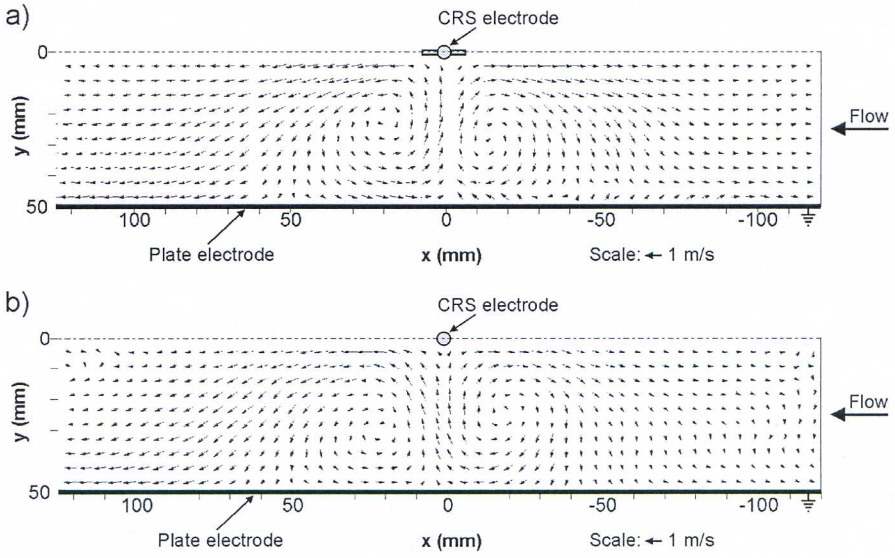


Fig. 3. Flow velocity field in the CDRS non–thermal plasma reactor at a main flow velocity of 0.2 $m\,s^{-1}$. Positive polarity, discharge current 150 μA, additional gas flow 0.5 $l\,min^{-1}$. a) the observation plane through the nozzle, b) the observation plane between the two nozzles.

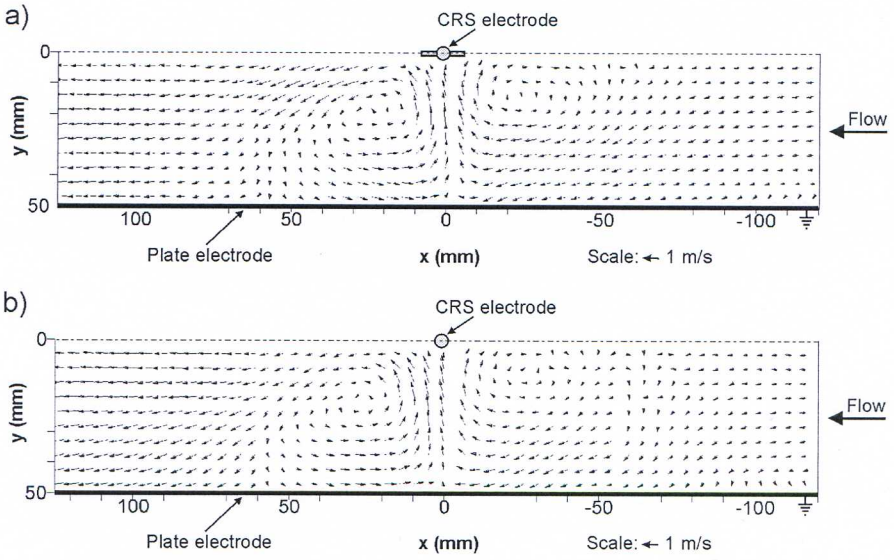


Fig. 4. Flow velocity field in the CDRS non–thermal plasma reactor at a main flow velocity of 0.4 $m\,s^{-1}$. Positive polarity, discharge current 150 μA, additional gas flow 0.5 $l\,min^{-1}$. a) the observation plane through the nozzle, b) the observation plane between the two nozzles.

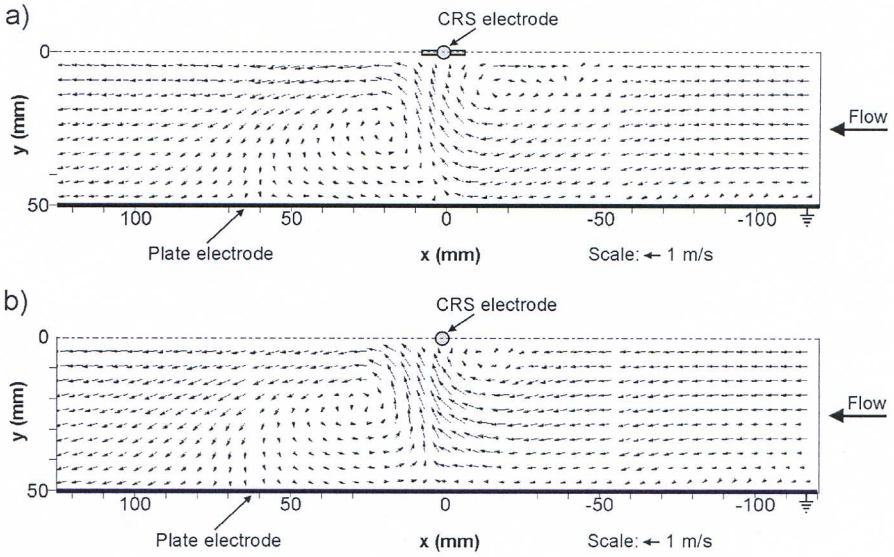


Fig. 5. Flow velocity field in the CDRS non–thermal plasma reactor at a main flow velocity of 0.6 $m\,s^{-1}$. Positive polarity, discharge current 150 μA, additional gas flow 0.5 $l\,min^{-1}$. a) the observation plane through the nozzle, b) the observation plane between the two nozzles.